RZ 3871 (#Z1209-002) 09/30/2012
Physical Sciences 18 pages

Research Report

Bond Order Discrimination by Atomic Force Microscopy

Leo Gross[1], Fabian Mohn[1], Nikolaj Moll[1], Bruno Schuler[1], Alejandro Criado[2], Enrique Guitián[2], Diego Peña[2], André Gourdon[3], and Gerhard Meyer[1]

[1]IBM Research - Zurich, CH-8803 Rüschlikon, Switzerland

[2]CIQUS, Universidade de Santiago de Compostela, E-15782 Santiago de Compostela, Spain

[3]CEMES-CNRS, F-31055 Toulouse Cedex, France

Research
Almaden • Austin • Brazil • Cambridge • China • Haifa • India • Tokyo • Watson • Zurich

Bond Order Discrimination by Atomic Force Microscopy

Leo Gross[1,*], Fabian Mohn[1], Nikolaj Moll[1], Bruno Schuler[1], Alejandro Criado[2], Enrique Guitián[2], Diego Peña[2], André Gourdon[3], and Gerhard Meyer[1]

[1] IBM Research - Zurich, CH-8803 Rüschlikon, Switzerland

[2] CIQUS, Universidade de Santiago de Compostela, E-15782 Santiago de Compostela, Spain

[3] CEMES-CNRS, F-31055 Toulouse Cedex, France

*To whom correspondence should be addressed. E-mail: lgr@zurich.ibm.com

We show that the different bond orders of individual carbon-carbon bonds in polycyclic aromatic hydrocarbons (PAHs) and fullerenes can be distinguished using noncontact atomic force microscopy (NC-AFM) with a CO-functionalized tip. Two different contrast mechanisms were found, which were corroborated by density functional theory calculations: The greater electron density in bonds of higher bond order led to a stronger Pauli repulsion, which enhanced the brightness of these bonds in high-resolution AFM images. The apparent bond length in the AFM images decreased with increasing bond order because of tilting of the CO molecule at the tip apex.

Bond order is an important concept to predict geometry, stability, aromaticity, reactivity, and electronic structure of covalently bonded molecules. The bond order is closely related to the bond length, which in general decreases with increasing Pauling bond order (*1*, *2*). If single crystals are available, the bond length can be determined experimentally with high accuracy using diffraction methods, which e.g. in the case of fullerenes (C_{60}), as predicted by Clar's sextet theory, showed two kinds of bonds of different lengths (*3*-*6*). In contrast to diffraction-based techniques, which yield values averaged over large ensembles of molecules, scanning probe microscopy offers the possibility to study single bonds in individual molecules.

Recently, rapid progress has been reported in the field of noncontact atomic force microscopy (NC-AFM), including the chemical identification of individual surface atoms (*7*), atomic resolution of carbon nanotubes (*8*), C_{60} (*9*), and planar organic molecules (*10*). For molecules, not only the chemical species of their constituent atoms can differ, but also the coordination number of atoms, the bond angles, and the bond order and bond length. In PAHs, the differences in bond order and length are subtle, but detecting them is useful for rationalizing aromaticity and reactivity of such molecules (*11*). AFM offers the possibility to study systems where single crystals needed for diffraction methods cannot be grown. Moreover, bond order determination within individual molecules is desirable for chemical structure determination (*12*), for the investigation of isomerization reactions where bond order changes (*13*, *14*), and for the characterization of structural relaxations around atomic defects in graphene (*15*-*17*).

We demonstrate an AFM method to differentiate bond orders and lengths of individual bonds for C_{60} and large PAHs, and investigated C-C bonds parallel to the sample surface. Hence, differences in contrast arising from the chemical species of the atoms (*12, 18*) or variations of the tip-sample separation (non-planar adsorption geometries) (*12, 19*) can be neglected. In a C_{60} molecule, the bonds fusing two hexagons (*h*) are electron-rich compared to the bonds fusing a pentagon and a hexagon (*p*), see Fig. 1A. The Pauling bond order P_b of a bond *b* in a conjugated molecule is found by counting the number of Kekulé structures (classical resonance formulas) that show *b* as a double bond divided by the total number of different Kekulé structures of the molecule (*1, 2*). Thus, P_b can take values between 0 (single bond) and 1 (double bond), and in the case of C_{60} the Pauling bond orders are $P_h = 0.44$ and $P_p = 0.28$, respectively (*20*). Correspondingly, theoretical (*21*) and experimental investigations using neutron diffraction (*3*), electron diffraction (*4*), and X-ray diffraction (*5, 6*) have shown that the bond *h* is shorter than the bond *p* by about 5%. The measured bond lengths are $L_h = 1.38(2)$ Å and $L_p = 1.454(12)$ Å, respectively (*22*).

We used a combined scanning tunneling microscopy (STM)/AFM system equipped with a qPlus force sensor (*23*) operating at 5 K and imaged the molecules with CO-functionalized tips (*10, 12, 24, 22*). The exact molecular adsorption orientation of C_{60} on Cu(111) was determined by STM (*25, 26*) (inset in Fig. 1A). The molecule shown in Fig. 1 exhibited a hexagonal tile and is oriented as depicted in Fig. 1A. Using NC-AFM, we recorded the frequency shift Δf at constant tip height *z* (*22, 27*), shown in Fig. 1B-E. To obtain atomic contrast, *z* had to be decreased, usually until $\Delta f(z)$ reached its minimum

above the molecule (in general at about z = 3.9 Å) and the contrast increased as z was further decreased. The smallest tip height where stable imaging conditions could still be maintained was $z \approx 3.3$ Å, see Fig. 1E. The origin of the atomic contrast is Pauli repulsion, which increases with the local electron density, giving rise to the bright features corresponding to the atomic structure of the imaged molecule. The dark halo surrounding the molecules in the AFM images stems mainly from the attractive van der Waals (vdW) force, which shows no corrugation on the atomic scale (*10, 28*).

Two striking observations can be made from the AFM images in Fig. 1. On the one hand, Δf is increased above the *h* bonds with respect to the *p* bonds. This effect was best observed for moderate tip heights, i.e., in Fig. 1B. As can be read off in Fig. 1G by comparing the two local maxima of a line profile $\Delta f(x)$ across both bonds, the largest Δf difference of about 0.4 Hz was observed for z = 3.7 Å. Moreover, in images with atomic resolution the *h* bonds appear shorter compared to the *p* bonds, which was best observed for the smallest accessible tip heights, i.e., in Fig. 1, D and E. Figure 1F shows a Laplace filtered image that was used to determine the apparent position of the bonds and to measure the apparent bond length, L'_h = 2.0(2) Å and L'_p = 2.7(2) Å, respectively (*22*). Remarkably, the apparent bond lengths L' measured by AFM qualitatively correctly reflect that the *h* bond is shorter than the *p* bond. However, both bonds appear significantly longer than they really are, and the difference in the apparent bond lengths of about 30% is much greater than the real difference of about 5%.

To understand the contrast mechanisms, density functional theory (DFT) calculations were performed (*22*). Fig. 2A shows an image of the calculated interaction energy for a CO tip at a tip height of d = 2.9 Å, which can be qualitatively compared to the Δf image at z = 3.8 Å (Fig. 1B) (*22*, *27*, *29*). The brighter appearance of the *h* bonds with respect to the *p* bonds is well reproduced. The contrast is related to the electron density (shown in Fig. 2B), which increases with bond order. The higher electron density leads to stronger Pauli repulsion and in consequence Δf is increased above bonds with greater bond order.

To take tip relaxations, especially tilting of the CO molecule at the tip apex (*30, 31*), into account, we modeled the tip as a Cu_2 cluster with a CO molecule attached as shown schematically in Fig. 2C (*22*). Calculated $\Delta f(x)$ line profiles (Fig. 2D) without relaxations of the tip structure (dashed lines) show the $\Delta f(x)$ maxima above the bond positions (vertical gray lines), reflecting the corrugation of the C_{60} electron density. Calculations including tip relaxations (solid lines) show a lateral shift of the $\Delta f(x)$ maxima positions toward greater absolute values of x, leading to an expansion of the molecule in the image. Moreover, this lateral shift is greater above the *h* bond compared to the *p* bond in agreement with the experiment. The important tip relaxation for the imaging process is the lateral displacement $\Delta x(x)$ of the oxygen atom at the tip apex (Fig. 2E) caused by the tilting of the CO toward the molecular center because of lateral forces. As this oxygen atom defines the position of our probe, a falling slope of $\Delta x(x)$ results in an expansion, while a rising slope of $\Delta x(x)$ results in a compression along the x direction in the particular region of the image. The absolute value of Δx is greater above the *h* bond compared to the *p* bond (see Fig. 2E). Hence the *h* bond appears shifted further away

from the molecular center than the *p* bond (see Fig. 2D), resulting in a decrease of L'_h with respect to L'_p as observed in the experiment.

Thus, the tilting of the CO is responsible for the amplification of the differences in apparent bond length with respect to the real differences in bond length. Note that, only because of this amplification, differences in apparent bond length can be measured within the accuracy of the AFM instrument. Furthermore, right above the apparent positions of the bonds, that is, when the regions of maximal electron density are probed, $\Delta x(x)$ takes a rising slope, thus leading to a local lateral compression, which gives rise to the very sharp appearance of the bonds at small tip heights. Remarkably, the calculations for d = 3.4 Å reflect also several other details of the experiment, such as the appearance of a local maximum in the molecular center and the vanishing Δf contrast between *p* and *h* bonds observed for very small tip heights due to the tip relaxations.

Next, we investigated the PAHs hexabenzo(*bc,ef,hi,kl,no,qr*)coronene (HBC) on Cu(111) and dibenzo(*cd,n*)naphtho(3,2,1,8-*pqra*)perylene (DBNP) (*32*) on bilayer NaCl on Cu(111) (*33*). In general, the bonds at the periphery of a planar molecule show an increased frequency shift Δf corresponding to greater repulsive forces compared to bonds in the central region (*28*). In part, this effect is related to the delocalization of electrons in a π-conjugated system leading to increased electron density at the boundary. In addition, the smaller attractive vdW background at the periphery of the molecule leads to an increased Δf compared to the central molecular region. Because these effects are not easily deconvolved from contrast related to bond order differences, we focused on bonds

in the central region of the molecules. Note that bond order differences are obscured by the vdW background in the case of pentacene (*10, 28*) where all bonds are near the periphery of the molecule. For HBC, see model in Fig. 3A, the bonds *i* and *j* are not connected to the periphery and the bonds within the central ring *i* are of greater bond order than the bonds *j* connecting the central ring to the outside rings (*35*). The qualitative contrast related to the bond order that was described above for C_{60} is corroborated for HBC. In particular, we observed that bonds with increased bond order appear brighter for moderate tip heights, see Fig. 3B and Fig. S1 and S2 (*22*), and the differences in bond length were qualitatively reflected and amplified in the regime of minimal tip heights, see Fig. 3C. The two different bonds *i* (P_i = 0.4, L_i = 1.417(2) Å) and *j* (P_j = 0.2, L_j = 1.447(2) Å) (*35*) were differentiated in the Δf contrast at constant height, shown in Fig. 3B, measured as Δf_i = -5.34(4) Hz, and Δf_j = -5.46(6) Hz, respectively. The differences in apparent length could be observed in Fig. 3C and were measured as L'_i = 1.48(4) Å and L'_j = 1.68(7) Å, with the errors corresponding to the standard deviation measured for all six equivalent bonds, see Fig. S3 (*22*). As described above, the contrast can be related to the calculated electron density, shown in Fig. 3D, which qualitatively reproduces the measured differences in Δf (Fig. 3B). Remarkably, we can distinguish individual *i* and *j* bonds although they differ only by 0.03 Å in length.

Finally, we investigated DBNP, a PAH that contains bonds of several different bond orders. The five bonds in the central molecular region (labeled *q*-*u* in Fig. 4A) have Pauling bond orders ranging from P_t = 0.163 to P_r = 0.49. Using both contrast mechanisms described above, we could assign *r* as the bond of comparably highest bond

order (*33*). Out of these five bonds, it showed the largest Δf signal (Fig. 4B and D) and the smallest apparent length (Fig. 4C and E). For the remaining four bonds, the differentiation was less clear, as can be seen in the graphs in Fig. 4D and Fig. 4E. Note that for DBNP, the bond order assignment was more challenging because of its low symmetry.

From our measurements on all three investigated molecular species, we can conclude that Pauling bond order differences between individual bonds down to about 0.2 can be distinguished using NC-AFM by both described contrast mechanisms. The frequency shift measured in different experimental runs can not be compared quantitatively because of different background contributions of different tips. However, the measured apparent length showed no tip dependence within the experimental errors as long as a stable CO-functionalized tip was used. Thus, the apparent lengths measured with different tips and on different planar (34) molecules can be compared as shown for HBC and DBNP in Fig. 4E. In Fig. 4F, the apparent length is plotted as a function of the realistic bond length extracted from DFT calculations (for DBNP) (*22*) and X-ray diffraction measurements (HBC) (*35*). The slope of the linear regression is 11, i.e., the differences of the apparent bond length are about an order of magnitude greater than the differences in real bond length, as a result of the CO tilting at the tip apex. The two contrast mechanisms, one based on the frequency shift and the other based on the apparent length measured by AFM, are both corroborated by DFT calculations and both can be used to differentiate bond orders in individual molecules. Remarkably, tilting of the CO at the tip apex

amplifies the apparent length differences and renders it possible to detect length differences between individual bonds down to 0.03 Å.

References and Notes

(1) L. Pauling, L. O. Brockway, J. Y. Beach, *J. Am. Chem. Soc.* **57**, 2705 (1935).

(2) J. Sedlar, I. Andelic, I. Gutman, D. Vukicevic, A. Graovac, *Chem. Phys. Lett.* **427**, 418 (2006).

(3) W. I. F. David, *et al.*, *Nature* **353**, 147 (1991).

(4) K. Hedberg, *et al.*, *Science* **254**, 410 (1991).

(5) P. J. Fagan, J. C. Calabrese, B. Malone, *Science* **252**, 1160 (1991).

(6) S. Liu, Y. J. Lu, M. M. Kappes, J. A. Ibers, *Science* **254**, 408 (1991).

(7) Y. Sugimoto, *et al.*, *Nature* **446**, 64 (2007).

(8) M. Ashino, A. Schwarz, T. Behnke, R. Wiesendanger, *Phys. Rev. Lett.* **93**, 136101 (2004).

(9) R. Pawlak, S. Kawai, S. Fremy, T. Glatzel, E. Meyer, *ACS Nano* **5**, 6349 (2011).

(10) L. Gross, F. Mohn, N. Moll, P. Liljeroth, G. Meyer, *Science* **325**, 1110 (2009).

(11) P. von Ragué Schleyer, *Chem. Rev.* **101**, 1115 (2001).

(12) L. Gross, *et al.*, *Nature Chem.* **2**, 821 (2010).

(13) M. J. Comstock, *et al.*, *Phys. Rev. Lett.* **99**, 038301 (2007).

(14) M. Alemani, *et al.*, *J. Am. Chem. Soc.* **128**, 14446 (2006).

(15) K. S. Novoselov, *et al.*, *Science* **306**, 666 (2004).

(16) M. M. Ugeda, *et al.*, *Phys. Rev. Lett.* **107**, 116803 (2011).

(17) H. Wang, *et al.*, *Nano Lett.* **12**, 141 (2012).

(18) C.-S. Guo, M. A. Van Hove, R.-Q. Zhang, C. Minot, *Langmuir* **26**, 16271 (2010).

(19) N. Pavlicek, *et al.*, *Phys. Rev. Lett.* **108**, 086101 (2012).

(20) S. Narita, T. Morikawa, T. Shibuya, *J. Mol. Structure (Theochem)* **532**, 37 (2000).

(21) M. Bühl, A. Hirsch, *Chem. Rev.* **101**, 1153 (2001).

(22) Supplementary materials are available on *Science Online*.

(23) F. J. Giessibl, *Appl. Phys. Lett.* **76**, 1470 (2000).

(24) F. Mohn, L. Gross, G. Meyer, *Appl. Phys. Lett.* **99**, 053106 (2011).

(25) J. A. Larsson, *et al.*, *Phys. Rev. B* **77**, 115434 (2008).

(26) G. Schull, Y. J. Dappe, C. Gonzalez, H. Bulou, R. Berndt, *Nano Lett.* **11**, 3142 (2011).

(27) In the calculations d denotes the distance between the O atom of the unrelaxed tip (i.e. for $\Delta x = 0$) and the plane of the imaged atoms. In the experiment the tip height was measured with respect to the STM set point, therefore there is an offset with respect to d. Comparison with theory (*10, 28*) shows that the minimum of $\Delta f(d)$ above a carbon ring is usually found at $d = 3.9$ Å. By measuring the tip height that yielded the minimum of $\Delta f(z)$ in the experiment and by setting this height to $z = 3.9$ Å we determined the offset and we adjusted all other tip heights of a measurement series by applying the same offset. Therefore, the experimental z values correspond to the theoretical d values and approximately reflect the atomic tip-sample separation.

(28) N. Moll, L. Gross, F. Mohn, A. Curioni, G. Meyer, *New J. Phys.* **12**, 125020 (2010).

(29) F. Mohn, L. Gross, N. Moll, G. Meyer, *Nature Nanotech.* **7**, 227 (2012).

(30) Z. Sun, M. P. Boneschanscher, I. Swart, D. Vanmaekelbergh, P. Liljeroth, *Phys. Rev. Lett.* **106**, 046104 (2011).

(31) J. Welker, F. J. Giessibl, *Science* **336**, 444 (2012).

(32) A. Criado, D. Peña, A. Cobas, E. Guitián, *Chem. Eur. J.* **16**, 9736 (2010).

(33) C_{60} and HBC could not be stably imaged by AFM on NaCl films with atomic resolution because they were laterally manipulated when using small tip heights. In contrast, DBNP could be imaged on bilayer NaCl on Cu(111) and was investigated on this surface to demonstrate that bond order discrimination is possible on different substrates.

(34) As vdW background forces also induce significant tilting of the CO tip, the apparent bond length can only be compared if the vdW background is constant, which is given in the central part of planar molecules. The bond length measured for C_{60} cannot be compared to the bond length measured for planar molecules, because the vdW background is not constant in the region around the *p* and *h* bonds due to the spherical shape of C_{60}, resulting in additional lateral distortions. However, the *p* and *h* bonds can be compared to each other because of their similar vdW background..

(35) R. Goddard, M. W. Haenel, W. C. Herndon, C. Krueger, M. Zander, *J. Am. Chem. Soc.* **117**, 30 (1995).

(36) L. Bartels, G. Meyer, K.-H. Rieder, *Appl. Phys. Lett.* **71**, 213 (1997).

(37) T. R. Albrecht, P. Grütter, D. Horne, D. Rugar, *J. Appl. Phys.* **69**, 668 (1991).

(38) V. Blum, *et al.*, *Comp. Phys. Comm.* **180**, 2175 (2009).

(39) J. P. Perdew, K. Burke, M. Ernzerhof, *Phys. Rev. Lett.* **77**, 3865 (1996).

(40) A. Tkatchenko, M. Scheffler, *Phys. Rev. Lett.* **102**, 073005 (2009).

Acknowledgements:

Comments from R. Allenspach, J. Repp, and A. Curioni and financial support from EU projects ARTIST (Contract No. 243421), HERODOT (Contract No. 214954), the ERC advanced grant CEMAS, the Spanish Ministry of Economy and Competitiveness

(MINECO, CTQ2010-18208), Xunta de Galicia (10PXIB2200222PR) and FEDER is gratefully acknowledged.

FIGURE 1

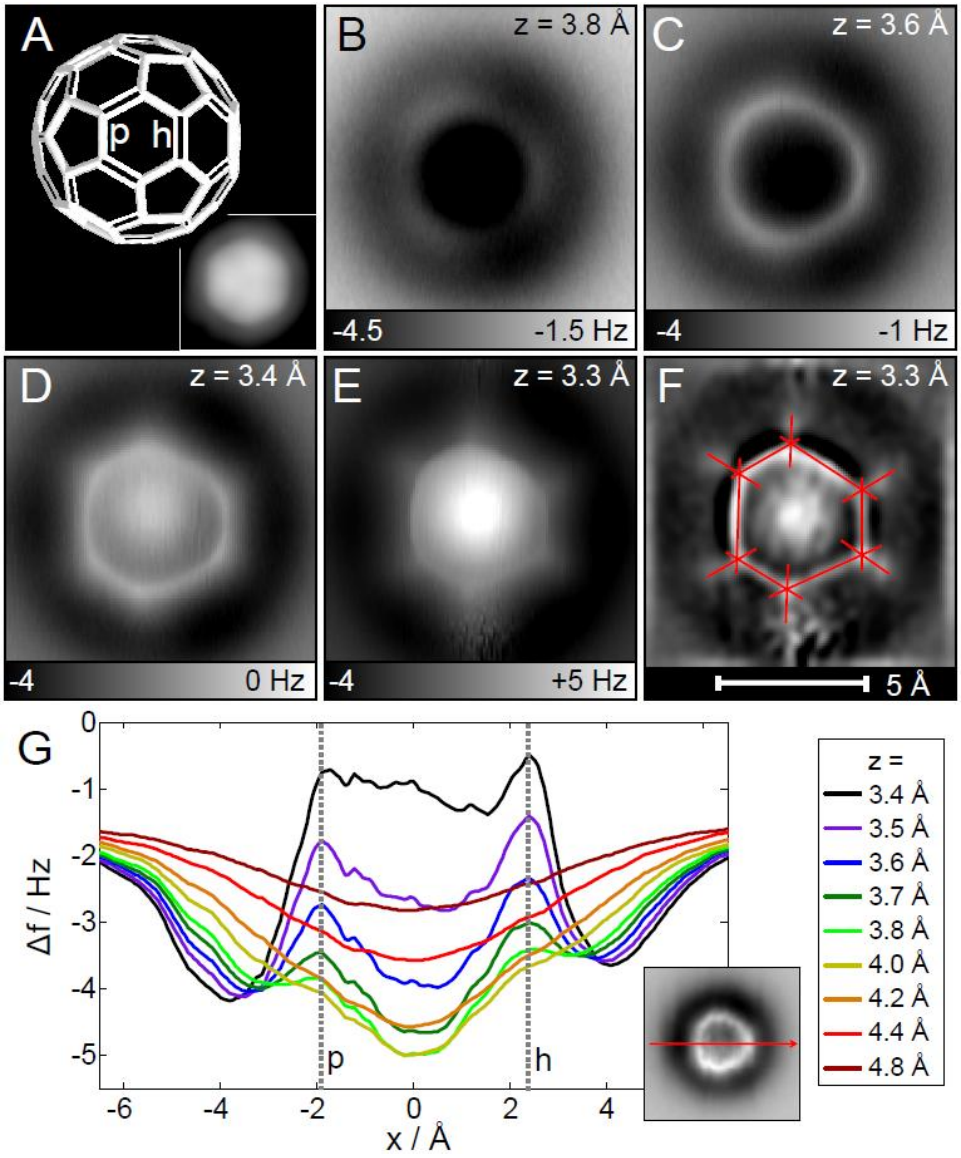

Figure 1. Measurements on C_{60}. (A) C_{60} model. The bonds fusing a pentagon and a hexagon (*p*) are of smaller bond order compared to the bonds fusing two hexagons (*h*). Inset: STM image (sample bias V = 0.2 V, current I = 2 pA, size 24 × 24 Å^2), molecule and tip are identical to (B)-(F). (B-E) AFM measurements showing Δf at different tip heights z (*27*) above C_{60}/Cu(111) using a CO-functionalized tip. Image size 10 × 10 Å^2,

oscillation amplitude A = 0.36 Å, V = 0 V. (F) Laplace-filtered and flattened image of (E), used to measure the apparent bond length L' (*22*). (G) Line profiles $\Delta f(x)$ across a *p* and *h* bond extracted from a 3D force map (*24*). The position of the line profiles is indicated in the inset, showing a map of Δf at z = 3.6 Å, extracted from the same 3D force map. The apparent positions of the *p* and *h* bonds are indicated by the dotted lines. The x = 0 position corresponds to the molecular center, determined by the minimum of $\Delta f(x)$ at z = 4.8 Å. Note that *p* is located at a smaller absolute value of x than *h* and note that $\Delta f(x_p)$ is smaller than $\Delta f(x_h)$ for all plotted values of z, with the maximum difference for z = 3.7 Å.

FIGURE 2

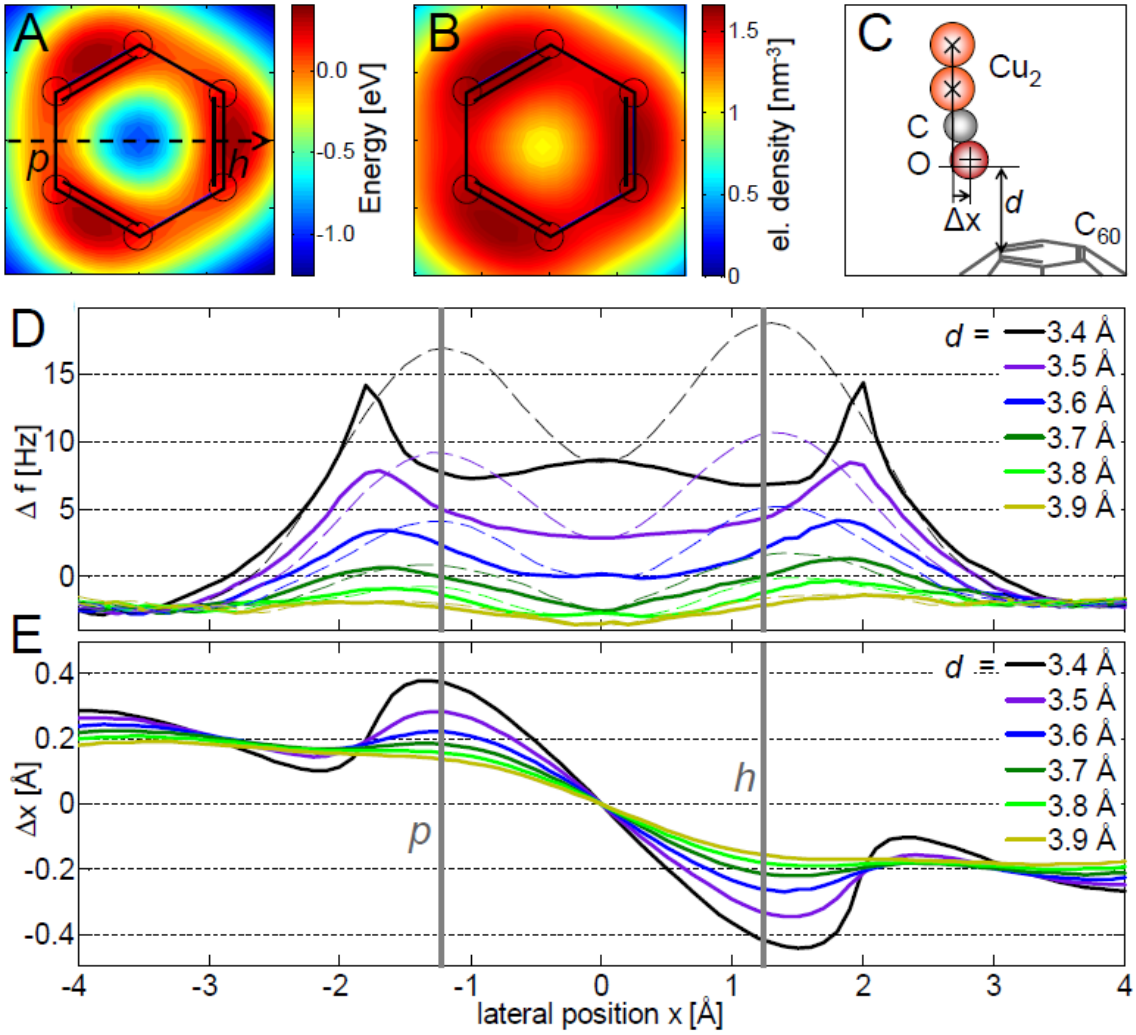

Figure 2. DFT calculations on C_{60}. Calculated interaction energy between CO and C_{60} at d = 2.9 Å (A) and electron density of C60 at 2.9 Å above the molecule (B), image size 4 × 4 Å^2. Using the tip model shown in (C), $\Delta f(x)$ line profiles along the dashed arrow in (A) were calculated with (solid lines) and without (thin dashed lines) relaxing the tip geometry, respectively (D). The relaxation resulted in a lateral displacement of the oxygen atom $\Delta x(x)$, shown in (E). The vertical gray lines in (D) and (E) indicate the positions of the *p* and *h* bonds as expected from the atomic model.

FIGURE 3

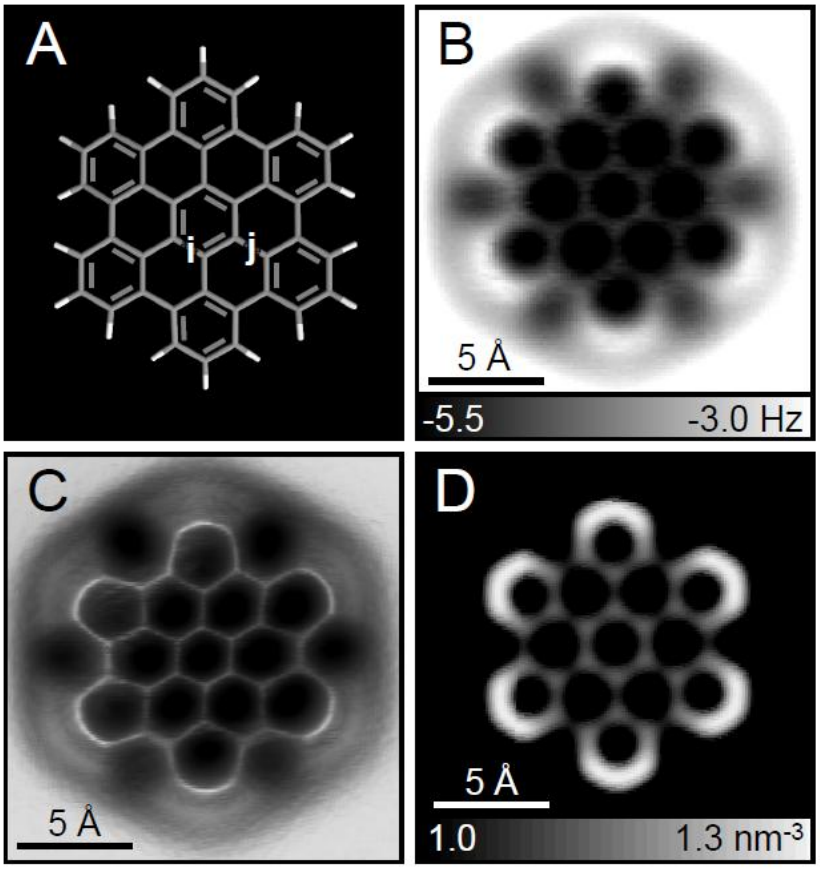

Figure 3. HBC. Hexabenzocoronene (HBC) model (A) and constant height AFM measurements (A = 0.35 Å) on HBC on Cu(111) at z = 3.7 Å (B), and z = 3.5 Å (C). In (C) a pseudo 3D representation is shown to highlight the local maxima. (D) Calculated electron density at a distance of 2.5 Å above the molecular plane. Note that *i* bonds are imaged brighter (B) and shorter (C) compared to *j* bonds (*22*).

FIGURE 4

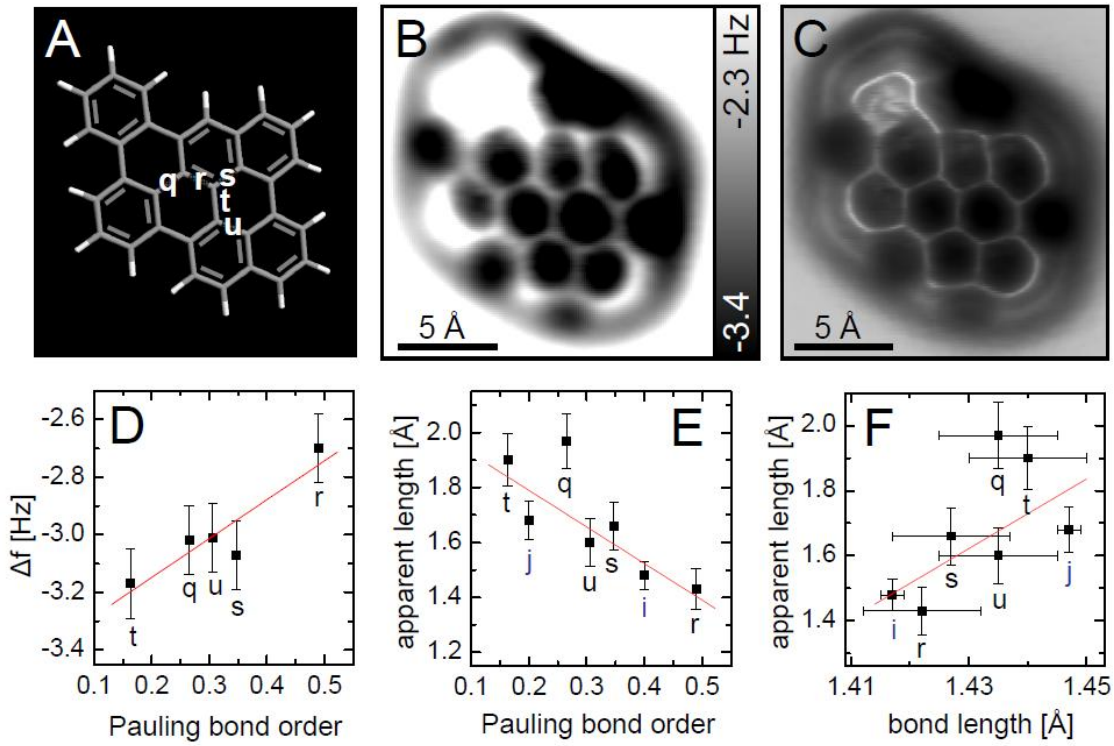

Figure 4. DBNP. Model (A) and constant height AFM measurements of DBNP on bilayer NaCl on Cu(111) (*33*) at z = 3.6 Å (A = 0.48 Å) (B, C). A pseudo 3D representation of (B) is shown in (C) to highlight the bonds. Measured values of the frequency shift Δf (D) and the apparent bond length L' (E) for indicated bonds, including HBC in (E) are plotted as a function of the Pauling bond order. (F) Apparent bond length as a function of the realistic bond length obtained by DFT calculations (for DBNP) (*22*) and from diffraction data (for HBC) (*35*). Linear regressions are drawn as a guide to the eye.